Solution Structure and Interaction of Cupiennin 1a, a Spider Venom Peptide, with Phospholipid Bilayers[†]

Tara L. Pukala,[‡] Martin P. Boland,[§] John D. Gehman,[§] Lucia Kuhn-Nentwig,[||] Frances Separovic,*[,§] and John H. Bowie[‡]

Department of Chemistry, University of Adelaide, Adelaide, South Australia, 5005, Australia, School of Chemistry, University of Melbourne, Melbourne, Victoria, 3010, Australia, and Zoological Institute, University of Bern, CH-3012, Switzerland

Received November 7, 2006; Revised Manuscript Received December 18, 2006

ABSTRACT: The solution structure of cupiennin 1a, a 35 residue, basic antibacterial peptide isolated from the venom of the spider *Cupiennius salei*, has been determined by nuclear magnetic resonance (NMR) spectroscopy. The peptide was found to adopt a helix−hinge−helix structure in a membrane mimicking solvent. The hinge may play a role in allowing the amphipathic N-terminal helix and polar C-terminal helix to orient independently upon membrane binding, in order to achieve maximal antibacterial efficacy. Solid-state ^{31}P and ^{2}H NMR was used to further study the effects of cupiennin 1a on the dynamic properties of lipid membranes, using zwitterionic chain deuterated dimyristoylphosphatidylcholine (d_{54}-DMPC) and anionic dimyristoylphosphatidylglycerol (DMPG) multilamellar vesicles. In d_{54}-DMPC alone, cupiennin 1a caused a decrease in the ^{31}P chemical shift anisotropy, indicating some interaction with the lipid head groups, and a decrease in order over the entire acyl chain. In contrast, for the mixed (d_{54}-DMPC/DMPG) lipid system cupiennin 1a appeared to induce lateral separation of the two lipids as evidenced by the ^{31}P spectra, in which the peptide preferentially interacted with DMPG. Little effect was observed on the deuterated acyl chain order parameters in the d_{54}-DMPC/DMPG model membranes. Furthermore, ^{31}P NMR relaxation measurements confirmed a differential effect on the lipid motions depending upon the membrane composition. Therefore, subtle differences are likely in the mechanism by which cupiennin 1a causes membrane lysis in either prokaryotic or eukaryotic cells, and may explain the specific spectrum of activity.

Antibacterial peptides are widely distributed throughout nature and form an ancient and pervasive component of the innate immune system for invertebrates, vertebrates, plants, and even microbes themselves (*1*, *2*). Several hundred antimicrobial peptides have been characterized to date, and their sequences are available together with a comprehensive list of reviews and publications (*3*).

Since traditional antibiotic therapeutics target the receptors and enzymes that are components of the bacterial biochemical machinery, rapid adaptation has led to the emergence of a number of drug resistant bacterial strains, which is clearly a serious public health concern (*4*). The majority of antibacterial peptides appear to act via a specific, but not receptor-mediated, permeabilization of the target membrane (*5*−*8*). This confers considerable potential for the development of such peptides as novel therapeutic agents, in particular, those that preferentially lyse bacterial cell membranes. Hence there is much interest in understanding the mechanistic properties of antibacterial peptides and the factors that govern selectivity.

Although the sequences of antimicrobial peptides are enormously diverse, they can be broadly classified based on primary and secondary structures. By far the most abundant and well-studied are the linear helical peptides, which are generally short (<40 residues) and cationic, and adopt amphipathic α-helical structures in membrane environments (*9*). Typical examples of this group include the cecropins, magainins, and melittin (*5*). Several models have been proposed to account for the way in which these linear helical peptides interact with and disrupt the bacterial membrane, of which the barrel-stave and carpet mechanisms have been most widely applied. In the barrel-stave model, peptides aggregate at the membrane surface before inserting into the membrane via formation of a transmembrane pore (*10*−*12*). For the carpet mechanism, peptides assemble parallel to the membrane surface, forming a detergent-like monolayer (*8*, *13*, *14*). Regardless of the mode of penetration, ultimately the disruption of normal membrane function results in cell lysis.

Arthropod venom has been identified as a rich source of antibacterial peptides, the vast majority of which conform to the linear helical classification, and are thought to play a role in protecting the venom apparatus against infection (*15*). Interestingly, however, these peptides display limited specificity, with many having the added ability to lyse erythrocytes, and also directly affect neuronal cell membrane potential (*15*−*18*). This general cytolytic activity suggests a

[†] The authors thank the Australian Research Council for the financial support of this project.

* Correspondence to this author: School of Chemistry, Bio21 Institute, University of Melbourne, Victoria, 3010, Australia. Tel: +61 3 8344 2447. Fax: +61 3 9347 5180. E-mail: fs@unimelb.edu.au.

[‡] University of Adelaide.

[§] University of Melbourne.

[||] University of Bern.

10.1021/bi062306+ CCC: $37.00
Published on Web 02/24/2007

dual role for the antibacterial peptides, which often act synergistically with other neuropeptide components of the venom, to enhance the overall toxicity (*19*). The balance between antibacterial and cytolytic functions for such dual-role peptides depends upon the structural features of both the peptide and target membranes.

To date, a small range of cytolytic peptides have been described from the venom of spiders, and only for those of the *labidognatha* suborder (*15*). This includes cupiennin 1a, isolated from the venom of the neotropical wandering spider, *Cupiennius salei* (Ctenidae), a large nocturnal hunting spider distributed throughout the tropical rain forests of Central America (*19*−*21*). Cupiennin 1a, a 35 residue, basic peptide (sequence: GFGAL FKFLA KKVAK TVAKQ AAKQG AKYVV NKQME-NH_2), shows significant antibacterial activity toward both Gram-positive and Gram-negative bacteria, with minimum inhibitory concentrations (MIC[1]) between 0.3 and 5 μM (*21*). In addition, this peptide is cytolytic (MIC of 25 μM toward human erythrocytes) and insecticidal (LD_{50} of 5.9 pmol·mg^{-1} fly toward *Drosophila*) (*21*).

CD studies show that, despite being unstructured in aqueous solution, cupiennin 1a contains significant amounts of α-helical secondary structure when in a lipid environment (*20*, *21*). However, a helical net projection shows that cupiennin 1a has a unique amphipathic motif in which the N-terminus is connected by a spiral band of Lys and polar amino acids to the C-terminus (*20*, *21*). Furthermore, structure−activity relationship studies conducted previously for the natural analogue, cupiennin 1d, suggest that the hydrophobic N-terminal segment primarily determines the antibiotic effects and insecticidal properties of these peptides, while the polar C-terminus seems to modulate peptide accumulation at negatively charged cell surfaces via electrostatic interactions (*20*). Interestingly, the mean hydrophobicity values and hydrophobic moment of the cupiennin peptides are particularly low in comparison with other antimicrobial peptides and, therefore, either the hydrophobicity of the N-terminal region is sufficient to induce membrane disruption or the high activity is related to their unusual distribution of charged and hydrophobic residues. Consequently, we now report the structure of cupiennin 1a in a membrane-like environment using solution state NMR spectroscopy and restrained molecular dynamics calculations (*22*−*25*).

While the conformation of the peptide contributes to understanding antibacterial activity, it is also necessary to directly investigate the peptide−membrane interaction. For this purpose, solid-state NMR methods have been widely applied to model lipid membranes (*26*−*29*). Naturally abundant ^{31}P in the phospholipid head group and synthetically incorporated ^{2}H in the acyl chains provide probes for investigating motion in the respective portion of the lipid molecule, over a wide range of time scales. For example, the ^{2}H quadrupolar interaction can detect molecular motions in the order of approximately 10−100 kHz, and the ^{31}P chemical shift anisotropy (CSA) is effective for probing rates of 4−6 kHz (*29*). Furthermore, relaxation measurements can provide insight into lipid molecular motions occurring on the nano- to millisecond time scale (*28*, *30*−*32*). Solid-state NMR spectroscopy is, therefore, a useful method for studying the dynamics resulting from perturbation of the phospholipid bilayers by membrane active peptides.

In this study, the solution structure of cupiennin 1a has been determined in a membrane mimicking solvent mixture, trifluoroethanol/water (TFE/H_2O) (*21*). Furthermore, the effects of cupiennin 1a on the order and dynamic properties of lipid membranes were investigated using ^{31}P and ^{2}H solid-state NMR spectroscopy, in two model membrane systems representing eukaryotic (zwitterionic multilamellar vesicles (MLV) of dimyristoylphosphatidylcholine (DMPC) and prokaryotic (anionic MLV, DMPC/dimyristoylphosphatidylglycerol, DMPG) cells. The results presented here provide some insight into the mechanism by which cupiennin 1a exerts both cytolytic and antibacterial effects.

MATERIALS AND METHODS

Solution-State NMR Spectroscopy. The isolation, primary structure determination, and subsequent synthesis of cupiennin 1a have been described previously (*21*). Solution structure studies were carried out in aqueous TFE, with the sample prepared by dissolving cupiennin 1a (5.3 mg, 1.3 μmol) in d_3-TFE/H_2O (1:1 v/v, 0.7 mL), to give a final concentration of 2.0 mM and pH of 2.55.

A Varian (Palo Alto, CA) Inova-600 NMR spectrometer was used for acquisition of all NMR spectra, with a ^{1}H frequency of 600 MHz and a ^{13}C frequency of 150 MHz. Experiments were carried out at 25 °C, and referenced to the methylene protons of residual unlabeled TFE (3.918 ppm). Referencing of the ^{13}C dimension of the HSQC spectrum (*22*) was achieved using the $^{13}CH_2$ signal of TFE (60.975 ppm). Suppression of the water signal was typically accomplished by centring the transmitter frequency on this resonance, and applying low power presaturation from the proton transmitter during a 1 s relaxation delay between scans. Gradient methods for suppression were used in the DQF-COSY experiment (*33*).

High-resolution 1D ^{1}H NMR spectra were acquired for cupiennin 1a in aqueous TFE, with 0.038 Hz per point digital resolution. TOCSY, DQF-COSY, and NOESY experiments (*34*, *35*) were collected in the phase sensitive mode. Typically, 64 time-averaged scans were acquired per increment with a total of 200 increments for each experiment, and the FID in t_2 consisting of 2048 data points over a spectral width of 5795.4 Hz. The NOESY spectrum was acquired with a mixing time of 250 ms, while the TOCSY pulse sequence included an 80 ms MLEV-17 spin-lock (*34*). The HSQC experiment was recorded with an interpulse delay of $(1/2)J_{CH} = 3.6$ ms, corresponding to $J_{CH} = 140$ Hz. One hundred twenty-eight increments, each comprising 64 transients, were acquired over 2048 data points in the directly detected ^{1}H, F_2 dimension. A spectral with of 25 641.0 Hz was used in the ^{13}C, F_1 dimension.

[1] Abbreviations: CD, circular dichroism; CSA, chemical shift anisotropy; DMPC, 1,2-dimyristoyl-*sn*-glycero-3-phosphocholine; DMPG, 1,2-dimyristoyl-*sn*-glycero-3-[phospho-*rac*-(1-glycerol)]; DQF-COSY, double-quantum-filtered correlation spectroscopy; FID, free induction decay; HSQC, heteronuclear single-quantum coherence; LD_{50}, dose sufficient to kill 50% of exposed population; MAS, magic angle spinning; MIC, minimum inhibitory concentration; MLV, multilamellar vesicle; NMR, nuclear magnetic resonance; NOE, nuclear Overhauser effect; NOESY, nuclear Overhauser effect spectroscopy; PC, phosphatidylcholine; PG, phospho-*rac*-(1-glycerol); RMD, restrained molecular dynamics; SA, simulated annealing; TFE, trifluoroethanol; TOCSY, total correlation spectroscopy.

2D spectra were processed using Varian software (VNMRJ, version 1.1D). Data matrices were multiplied by a Gaussian function in both dimensions before zero-filling to 4096 data points prior to Fourier transformation.

Structure Calculations. ^{1}H resonances in the NOESY spectra were assigned using Sparky software (version 3.111) and a standard sequential assignment procedure (*35*). Each of the cross-peaks was integrated, and the volumes were converted to distance restraints using the method of Nilges et al. (*23*). For each symmetric pair of cross-peaks, the peak of larger volume was used. $J_{NH\alpha H}$ values were measured from the high-resolution 1D ^{1}H NMR spectrum, and dihedral angles were restrained as follows: $^3J_{NH\alpha H} < 5$ Hz, $\phi = -60° \pm 30°$, $5 < {}^3J_{NH\alpha H} < 6$ Hz, $\phi = -60° \pm 40°$. For $^3J_{NH\alpha H}$ values ≥ 6 Hz, ϕ angles were not restrained. The absence of resolved splitting for an NH resonance implies that its $^3J_{NH\alpha H}$ value is <5 Hz.

Structures were generated from random starting conformations using ARIA (version 1.2) (*36*) implemented with CNS (version 1.1) (*37*). The standard restrained molecular dynamics (RMD) and simulated annealing (SA) protocol was used, with floating stereospecific assignments employed (*38*). A single ARIA run consisted of eight iterations, using optimized parameters based on those described by Pari et al. (*39*). In the final iteration, 60 structures were calculated, from which the 20 with lowest potential energy were selected for analysis. Three-dimensional structures were viewed using the program MOLMOL (version 2k.2) (*40*).

Solid-State NMR Spectroscopy. Phospholipids were purchased from either Avanti Polar Lipids (Alabaster, AL) or Sigma (St. Louis, MO), and used without further purification. Cupiennin 1a (1 mg, 0.26 μmoles) was codissolved in a small amount of chloroform/methanol (1:1 v/v) with either DMPC (protonated and deuterated, DMPC/d_{54}-DMPC, 2:1 mole ratio) or DMPC/d_{54}-DMPC/DMPG (1:1:1 mole ratio) to give an overall lipid/peptide molar ratio of 40:1. The solvent was evaporated under a stream of N_2, and the samples were dried under vacuum for several hours to ensure complete solvent removal. The samples were then resuspended in 52 μL of water, and submitted to five cycles of freeze−thawing followed by vortex mixing until a viscous transparent gel was obtained. They were then transferred to a 5 mm NMR rotor for magic angle spinning (MAS) experiments, or a 5 mm NMR tube for static analysis. Control samples of "pure-DMPC" and "mixed DMPC/DMPG" were prepared in a similar manner without the addition of peptide.

All NMR experiments were performed on a Varian (Palo Alto, CA) Inova-300 spectrometer, using a 5 mm Doty (Columbia, SC) MAS probe. ^{31}P proton decoupled experiments were carried out at an operating frequency of 121.5 MHz, using a single 90° pulse for excitation, and were referenced to H_3PO_4 (0 ppm). Spectra were recorded at 30 °C, and typical operating parameters included a 3.8 μs 90° pulse, 2 s recycle delay, and 62.5 kHz spectral width. Generally, 12k scans were averaged and processed with 100 Hz of exponential line broadening. Deconvolution of static spectra into axially symmetric CSA and isotropic components was accomplished by straightforward nonlinear least-squares fitting of frequency-dependent intensities:

$$I(\omega) = (1 - \sum_a f_a)F_{iso} + \sum_a f_a(\sum_{\theta=0}^{\pi/2} P(\theta,c/a)\, F(\theta))$$

where F_{iso} is a Gaussian line shape function centered at the isotropic chemical shift and contributes a fraction f_{iso} of total intensity; axially symmetric lines were defined by Gaussians centered at $\omega(\theta) = (\delta_{||} - \delta_{\perp})\cos^2\theta + \delta_{\perp}$ (*41*) with an orientation and spheroid axis-ratio c/a dependent probability P (where c is the unique axis) (*42*) and with each axially symmetric component uniformly scaled further by respective fractional contributions f_a. While principal CSA components $\delta_{||}$ and $\delta_{\perp}$ were not explicitly constrained to a specific isotropic value during the fitting, the isotropic frequency observed in MAS experiments on the same samples correlated well to the fit values.

Deuterium spectra were recorded at 46.1 MHz using a quadrupolar-echo pulse sequence (*43*) over a spectral width of 200 kHz. Typical operating parameters included a 5 μs 90° pulse, 40 μs echo delay, and 0.4 s recycle delay. Generally, 150k scans were averaged and processed with 200 Hz exponential line broadening. Unoriented deuterium spectra of overlapping Pake patterns (*43*) were "dePaked" using single value decomposition (*43*) as well as a straightforward nonlinear least-squares approach. Numerical mechanics were facilitated by the Gnu Scientific Library v1.7 (*44*). Order parameters were calculated simply by measuring the quadrupolar splitting in the calculated 0°-oriented spectrum for each myristoyl-C^{2}H$_n$ acyl chain position and then dividing by 255 kHz (3/2 times the static coupling constant) (*43*).

^{31}P relaxation experiments were carried out under MAS conditions (typically 6 kHz). Longitudinal relaxation times (T_1) were measured using the inversion recovery pulse sequence with a recycle delay of 4 s and variable delay values between 1 ms and 3 s. Transverse relaxation times (T_2) were measured with a Hahn spin−echo experiment with echo delay values between 0.1 and 18 ms and echo times set to integer multiples of the rotor period. Relaxation times were determined by fitting a single exponential to peak intensity decay versus time. Root-mean-square of noise was measured from empty spectral regions and used as the error in peak intensity data.

RESULTS

Solution-State NMR Spectroscopy. CD spectra have been recorded previously for cupiennin 1a and suggest that this peptide is unstructured in water but adopts an α-helical conformation in a 1:1 v/v aqueous TFE mixture (*21*). Therefore, NMR studies were undertaken using this solvent system. NMR spectra were acquired for cupiennin 1a in aqueous TFE, and proton chemical shifts were assigned using standard sequential assignment methods (*25*) and a combination of NOESY, TOCSY, and COSY experiments. αC resonances were identified by direct investigation of the αH/αC region of a HSQC spectrum. These spectra and a summary of all assigned proton and αC resonances are given as Supporting Information. NMR structural analysis was also carried out in dodecylphosphocholine micelles (at a 40:1 lipid/peptide ratio, data not shown). The observed spectra and, therefore, the structure which cupiennin 1a is likely to adopt were similar in each media. However, final structures were calculated in TFE/H_2O since the data obtained was of higher quality.

The αH resonances demonstrate a distinct upfield shift from random-coil values (*45*) along the majority of the

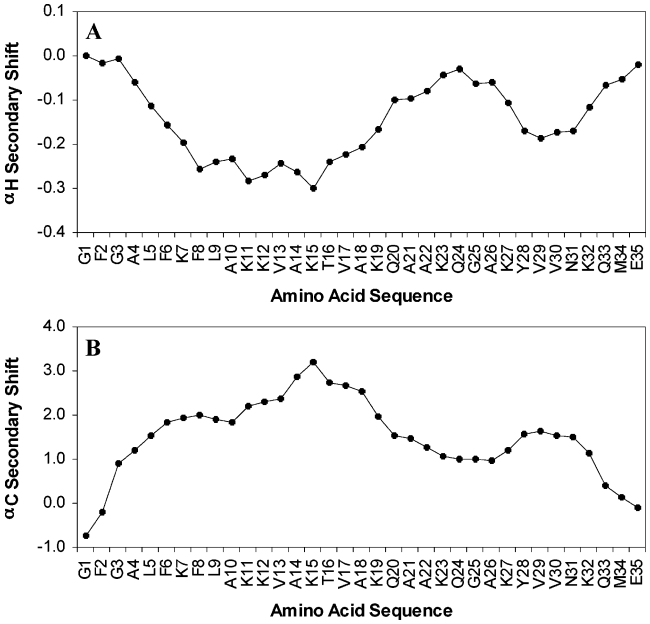

FIGURE 1: **(A)** αH ^{1}H and **(B)** αC ^{13}C secondary shifts of cupiennin 1a in TFE/H_2O, smoothed over $n \pm 2$ residues. Negative values indicate an upfield shift from random-coil resonances, while positive values indicate a shift downfield.

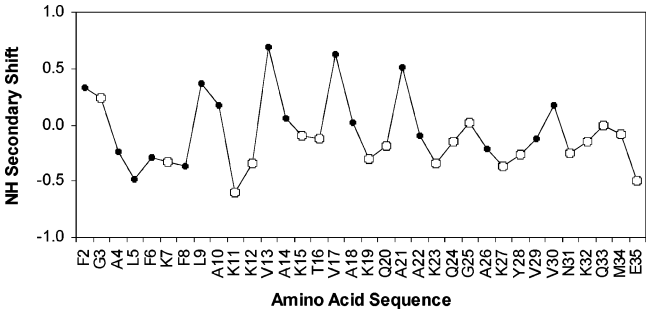

FIGURE 2: NH ^{1}H secondary shifts of cupiennin 1a in TFE/H_2O. Negative values indicate an upfield shift from random-coil values, while positive values indicate a shift downfield. Hydrophilic residues are represented by open symbols.

sequence (Figure 1A), consistent with the peptide having predominantly helical structure (*46*). The exception to this is in the vicinity of Gln24, and the N and C-termini, in which regions the resonances were more random-coil like. Although a lack of defined secondary structure is anticipated at the ends of the peptide due to a reduction in hydrogen bonding (*47*), the trend toward random-coil structure observed near the center of the peptide suggests that it adopts a helix−hinge−helix type conformation. This is further supported by the αC secondary shifts (Figure 1B), in which two distinct helical regions (encompassing residues 3−21 and 28−34) were identified by their significant downfield shift from random-coil values (*46*). NH secondary shift values deviate periodically over 3−4 residues, with hydrophobic residues generally producing resonances further downfield compared to those that are hydrophilic (Figure 2), characteristic of an amphipathic α-helix (*47*). The "zigzag" trend in the graph of NH secondary shifts is maximal between residues Lys7 and Ala22, suggesting that the amphipathicity is best defined in this region.

Diagnostic NOE connectivities for cupiennin 1a in TFE/H_2O are given in Figure 3. Here a strong series of d_{NN} signals are noted, in addition to a number of weaker $d_{NN(i,i+2)}$ NOEs.

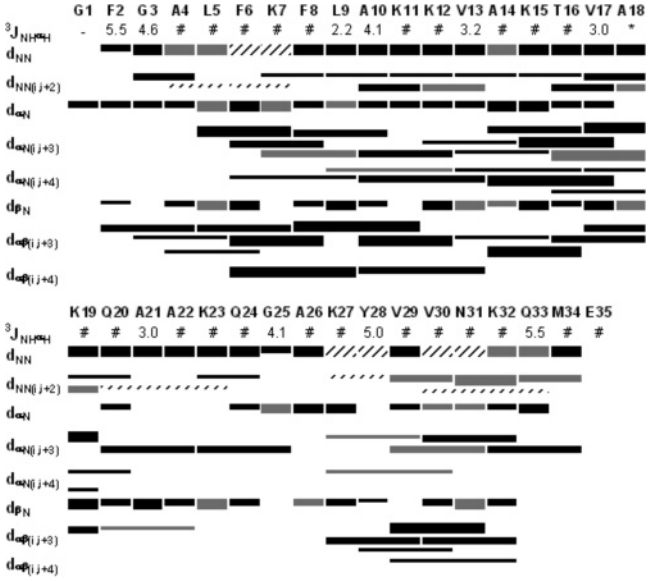

FIGURE 3: NOE connectivities of cupiennin 1a in TFE/H_2O. The thickness of the bars indicates the relative strength of the signal (strong <3.1 Å, medium 3.1−3.7 Å, weak >3.7 Å). Gray shaded boxes represent ambiguous NOEs, while striped boxes represent signals too close to the diagonal for clear observation. $^{3}J_{NH\alpha H}$ values are indicated where possible. ∗ indicates that no coupling constant was detected, while # indicates that the coupling constant could not be reliably assigned due to overlap.

Sequential $d_{\alpha N}$ and $d_{\beta N}$ NOEs also occur along most of the sequence. A significant number of medium range NOEs are present from 3 and 4 residues apart, particularly $d_{\alpha N(i,i+3)}$ $d_{\alpha N(i,i+4)}$ and $d_{\alpha\beta(i,i+3)}$ signals. No long-range NOE signals were observed, concordant with a lack of intermolecular association. The pattern of observed NOEs and their intensities is generally consistent with the peptide having helical structure along the majority of the sequence (*35*). However, the reduction in medium range NOEs in the region from A21 to A26 is further support for a helix−hinge−helix type structure in cupiennin 1a.

A total of 646 nonredundant distance restraints were generated from the NOESY spectrum of cupiennin 1a, of which 143 were ambiguous. Ten dihedral angle restraints were also employed during the structure calculations, derived from the $^{3}J_{NH\alpha H}$ coupling constants given in Figure 3. The conclusions drawn by examination of the NMR spectral data were confirmed by structural calculations, whereby 60 final structures were generated by the ARIA RMD and SA protocol, of which the 20 with lowest potential energy were chosen for analysis.

Figure 4 shows the 20 lowest energy structures of cupiennin 1a in TFE/H_2O, aligned over selected backbone residues. Superimposing the N-terminal helix (residues 3−21) led to a "fraying" of the C-terminal helix (residues 28−34). Similarly, superimposing the C-terminal helix caused the N-terminal helix to become indiscriminate. Clearly, cupiennin 1a adopts two well-defined helices, separated by a more flexible hinge region.

The energy and structural statistics for cupiennin 1a in TFE/H_2O are given in Table 1. Final structures demonstrated only minor deviation from idealized covalent geometry (≤0.05 Å for bonds, ≤5° for angles). Just seven distance restraints were violated at greater than 0.3 Å, suggesting that the resultant structures adequately satisfy the NMR derived

FIGURE 4: Twenty most stable calculated structures of cupiennin 1a in TFE/H_2O, superimposed over the backbone atoms of residues 3−21 (upper) and 28−34 (lower).

Table 1: Structural Statistics for Cupiennin 1a Following RMD/SA Calculations

energies (kcal·mol^{-1})	
E_{total}	25.45 ± 1.48
E_{bond}	0.38 ± 0.05
E_{angle}	12.35 ± 0.33
$E_{improper}$	0.75 ± 0.09
E_{VDW}	10.62 ± 1.09
E_{NOE}	1.33 ± 0.33
E_{cdih}	0.00
well-defined residues	3-21, 28−32
rmsd from mean geometry (Å)	
backbone atoms of well-defined residues (3−21)	0.85 ± 0.27
heavy atoms of well-defined residues (3−21)	1.34 ± 0.32
backbone atoms of well-defined residues (28−32)	0.21 ± 0.06
heavy atoms of well−defined residues (28−32)	1.18 ± 0.46
all backbone atoms	4.27 ± 1.11
all heavy atoms	5.17 ± 1.18

data and are likely to be an accurate representation of the peptide in solution. Rmsd values were calculated for the structure ensemble over the entire peptide and are also given in Table 1. The rmsd for the helical domains indicated that the structures in these two well-defined regions agreed very well with each other. A Ramachandran plot of the average ϕ and ψ angles for cupiennin 1a shows that the majority of residues fall within the favored region for α-helical structure (Supporting Information). Furthermore, residues Gly3−Ala21 as well as Tyr28−Lys32 were well-defined (angular order parameters (S) > 0.9 for both ϕ and ψ), but the remaining residues were poorly defined with low S values, particularly in the vicinity of Gln24 (Supporting Information). These data are all consistent with a helix−hinge−helix structure.

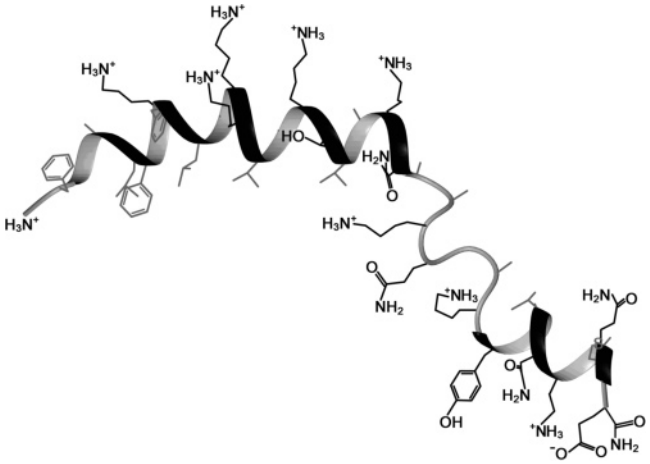

FIGURE 5: The lowest calculated potential energy structure of cupiennin 1a in TFE/H_2O.

The most energetically stable calculated structure of cupiennin 1a in TFE/H_2O (1:1 v/v) is shown in Figure 5. Here the helix−hinge−helix structure is clearly evident. This representation also shows that the N-terminal helix is amphipathic, with obvious hydrophobic and hydrophilic faces, while the C-terminus is essentially a hydrophilic helix.

^{31}P Solid-State NMR of Phospholipid Bilayers. Solid-state ^{31}P NMR is able to detect changes in the dynamics and orientation of the polar region of phospholipid molecules (*48*−*50*). The ^{31}P line shape or CSA of NMR spectra can reveal alteration of membrane topology or the membrane surface charge density (*51*, *52*), or more specific alignment and motion of the lipid head groups (*49*, *52*). Static ^{31}P spectra were collected for DMPC and DMPC/DMPG MLV, both with and without cupiennin 1a (Figure 6). The unoriented line shapes, which reflect axially symmetric CSA properties, indicate that the bilayers are in the fluid or liquid lamellar (L_α) phase (*48*). The ^{31}P CSA for DMPC MLV was approximately −47 ppm, in close agreement with previously reported data (*53*), and the CSA reduces to −39 ppm upon addition of cupiennin 1a.

The static line shape for mixed DMPC/DMPG MLV is consistent with a single axially symmetric ^{31}P tensor with CSA of −39 ppm. This CSA, typical of PC and PG head groups (*54*), is significantly smaller in magnitude than that of DMPC alone and suggests a lack of lateral phase separations in this binary lipid mixture under these conditions. Addition of cupiennin 1a to mixed DMPC/DMPG MLV has a profound effect on the ^{31}P line shape, with the signal revealing two contributing powder patterns. Deconvolution gave two liquid lamellar components with CSA widths of −40 and −25 ppm (Table 2) and respective fractional intensities suggestive of enriched but segregated DMPC and DMPG lipid domains.

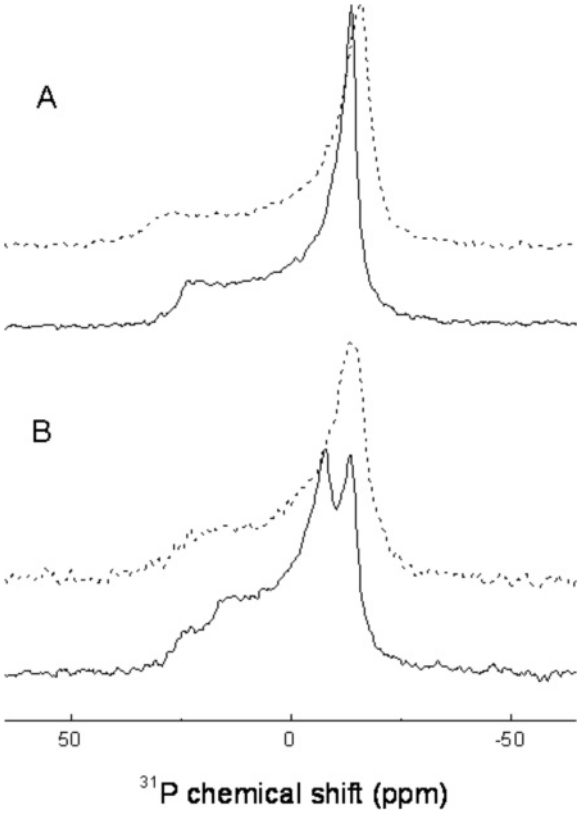

FIGURE 6: ^{31}P NMR spectra of **(**A**)** DMPC and **(**B**)** DMPC/DMPG (2:1) MLV at 30 °C, with and without cupiennin 1a (1:40). In each pair of spectra the dashed line represents the spectrum of the lipid sample, while the solid line represents the spectrum of the sample with cupiennin 1a.

^{2}H NMR of Phospholipid Bilayers. Static ^{2}H NMR spectra of chain-deuterated phospholipids are sensitive to the orientation and mobility of the lipid acyl groups (*55*−*57*). The ^{2}H spectra were typical of a fluid bilayer (*57*, *58*), with a small isotropic peak due to residual ^{2}H in the water (Supporting Information). The order parameters, as detailed in Materials and Methods, for each d_{54}-DMPC acyl chain position show little variation between typical values observed for control MLV samples (*59*−*61*) and those including peptide (Supporting Information).

^{31}P NMR Relaxation Studies. MAS allows the recording of high resolution solid-state ^{31}P NMR spectra where intensity from all orientations is averaged into a narrow peak at the isotropic chemical shift (*62*, *63*). The ^{31}P MAS spectrum of DMPC MLV with and without peptide gave a single narrow peak at −1.0 ppm while DMPC/DMPG revealed two resolved peaks at −0.9 and +0.2 ppm with intensities that reflect the molar ratio (i.e., 2:1) of each lipid (Figure 7); these peaks experience a slight upfield shift by 0.2 ppm when the peptide was included.

The ^{31}P MAS NMR relaxation times are reported in Table 2. T_1 and T_2 ^{31}P relaxation rates are sensitive to differential phospholipid head group mobility owing to an interaction of peptide with the membrane bilayer. T_1 relaxation pathways are driven by molecular motions on the nanosecond time scale, such as rapid conformational changes and long-axis lipid rotation (*29*, *31*, *64*). At lower fields, the T_1 of the phosphorus is predominantly determined by dipolar interactions with nearby protons and the motional model, both using the dipolar relation and incorporating anisotropic motions, showed that the measured T_1 accords with a correlation time of ∼1.4 ns, which represents the time constant of the ^{1}H−^{31}P interaction in a plane parallel to the bilayer surface (*64*). T_2 relaxation is driven by molecular motion on the millisecond time scale, such as diffusion of the lipid through the bilayer and collective membrane slow-order director fluctuations (*29*, *30*, *65*). Where relaxation times shorten upon addition of peptide, the peptide may be perceived to have increased the intensity of motions at corresponding frequencies. Conversely, where peptide lengthens relaxation times over control samples, the peptide may be perceived to have restricted motions at the corresponding frequencies. Addition of cupiennin 1a to pure DMPC caused a ∼15% decrease in T_1 and T_2. By contrast, cupiennin 1a imparted longer T_1 and T_2 relaxation times on both components of the mixed lipid MLV; T_1 times increased by ∼33%, while T_2 times increased by ∼10−20% for each component.

DISCUSSION

Solution NMR studies presented here demonstrate that cupiennin 1a adopts a predominantly α-helical structure in aqueous TFE, consisting of two helical domains separated by a distinct disordered region (Figure 5). TFE acts as a membrane mimicking solvent by promoting the formation of intramolecular hydrogen bonds (*66*, *67*), and therefore, it is likely that the calculated structures persist in a bilayer environment. This is supported not only by results of previous CD experiments, which show that the peptide adopts an α-helical structure in the presence of TFE or phospholipid vesicles (*20*, *21*), but also by the fact that NMR-derived conformations of a number of amphipathic α-helical peptides are similar in both TFE/H_2O and lipid bilayers (*66*, *68*, *69*). Furthermore, the observed helix−hinge−helix structure occurs frequently in cationic antimicrobial peptides, particularly those larger than 20 amino acids in length. Often the hinge is initiated by proline, or less commonly glycine residues, which are known to disrupt helical structure (*70*, *71*). Gly24 in the disordered region of cupiennin 1a may therefore contribute to the observed flexibility.

Earlier structural studies of cupiennin 1a describe a unique amphipathic motif, in which a right-handed ribbon of positively charged lysine resides winds around a presumed linear helix (*15*, *21*). However, in the NMR structure presented here, these positively charged residues describe a narrower grouping when the two α-helical regions are considered separately (lysine residues in both N- and C-terminal helices define an arc of 140°). Such an arrangement allows the N-terminal region to adopt an amphipathic conformation. In contrast, the C-terminal helix is essentially hydrophilic. As a result, it is likely that each helix has a different functional influence on the cytolytic activity of this peptide. Furthermore, the flexibility imparted by the central hinge would allow each helix to orient independently, thereby enhancing the membrane binding and permeabilizing ability of cupiennin 1a.

Structural, antibacterial, and hemolytic properties of truncated cupiennin 1a derivatives have been characterized by Kuhn-Nentwig et al. (*20*). Deletion of nine residues at the C-terminus causes a decrease in cytolytic efficacy, particularly toward Gram-positive bacteria, while additional elimination of the N-terminal pentapeptide entirely negates

Table 2: ^{31}P Data for DMPC and DMPC/DMPG MLV, with the Addition of Cupiennin 1a

	CSA (ppm)[a]		MAS isotropic shift (ppm)[b]		T_1 (ms)[c]		T_2 (ms)[d]	
+/− cupiennin 1a	−	+	−	+	−	+	−	+
DMPC MLV	−46.6	−39.4	−1.0	−1.0	1045	890	13.3	11.4
DMPC/DMPG MLV[e]	−40.5	−39.8 (68%)	−0.9 (65%)	−1.0 (66%)	538	697	6.1	6.8
		−25.3 (32%)	0.2 (35%)	0.0 (34%)	445	604	4.8	5.9

[a] CSA determined to ±0.5 ppm. [b] Chemical shift determined to ±0.02 ppm. [c] T_1 within ±20 ms. [d] T_2 within ±0.5 ms. [e] Component fractions of total intensity are given in parentheses.

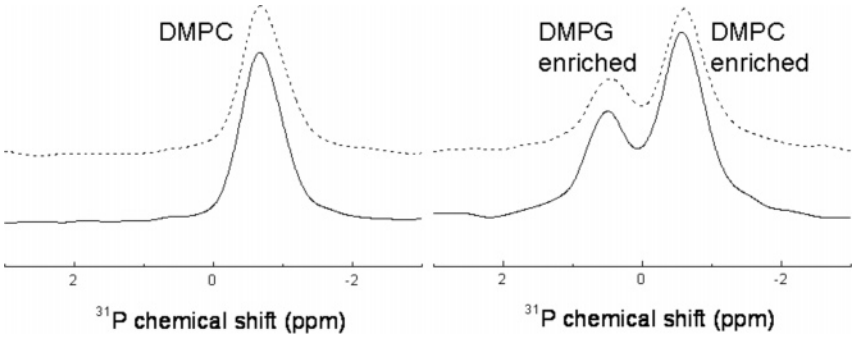

FIGURE 7: ^{31}P MAS NMR spectra of DMPC and DMPC/DMPG MLV at 30 °C. The dashed line represents the phospholipid alone, and the solid line with cupiennin 1a.

both antimicrobial and hemolytic activity. This is consistent with what is now known of the structure of cupiennin 1a, in that the cytolytic activity of the cupiennin peptides depends primarily on the amphipathic N-terminus, which is capable of inserting into the membrane, and is modulated by the C-terminus via electrostatic interactions with the cell surface (*20*).

Since cupiennin 1a is both antibacterial and hemolytic, solid-state NMR experiments were performed on net anionic phospholipid bilayers by using DMPC/DMPG to electrostatically model prokaryotic cell membranes and zwitterionic DMPC bilayers to model eukaryotic cell membranes. An important detail underlying the study is implicit in the static ^{31}P NMR data: MLV bilayers remain intact and maintain a liquid lamellar phase at 30 °C in the presence of cupiennin 1a at a lipid/peptide ratio of 40:1. The peptide appeared to maintain the same structure in dodecylphosphocholine micelles with a similar lipid molar ratio (NMR data not shown), and while the curvature is different, the α-helical structure is likely to be maintained in phospholipid bilayers. Although some peptides exhibit different helicities in detergent micelles and isotropic solvents (see, e.g., ref *68*), the α-helical structure is usually preserved. Likewise, the helicity of cupiennin 1a as determined by CD is maintained in small unilamellar vesicles, but it is higher in negatively charged compared to neutral phospholipids (*20*). Thus although the phospholipid charge may influence peptide structure, the amphipathic α-helical nature of cupiennin 1a would most likely be maintained for both MLV systems studied.

While the static ^{31}P spectrum of the mixed DMPC/DMPG MLV appeared to contain only one distinct liquid lamellar component, the two peaks differing by ∼1 ppm in the MAS spectra suggest that there are two components contributing to the static line shape. These two components have only subtly differing principal CSA elements, which, together with comparable relaxation rate constants, suggest little difference in the environment and motions experienced by each component. While the relative intensities of the major and minor components in the MAS spectra were consistent with the proportions of DMPC and DMPG, respectively, we can only safely assume that the major component, which appears at +0.1 ppm chemical shift relative to pure-DMPC MLV, is *enriched* with DMPC, and the minor component is enriched with DMPG, although there may be no segregation of enriched domains at all. These relative chemical shifts are consistent with reported correlation between upfield-shift of peak with decreasing negative membrane charge density (*51*, *52*).

The addition of cupiennin 1a to pure-DMPC MLV caused a narrowing of the CSA, and reductions in both T_1 and T_2, which could be a result of a change in motion, headgroup conformation, and/or correlation time. The presence of cupiennin 1a may have led to an increase in the motion experienced by the ^{31}P nucleus at all frequencies: in accord with the ∼15% decrease in T_1 (at $\sim 10^8$ Hz), CSA (corresponding to 10^3-10^4 Hz), and T_2 (low-frequency motions). Together with the lack of effect on the ^{2}H order parameters, the overall change in lipid dynamics would suggest that, if the peptide *has* inserted into the bilayer, there is little disruption of the bilayer integrity.

The addition of cupiennin 1a had largely the opposite effect on mixed DMPC/DMPG MLV, and appeared to discriminate between the DMPC-enriched and DMPG-enriched membrane components. The major, DMPC-enriched component of the ^{31}P static spectrum had a CSA value similar to the pure-DMPC MLV, while the CSA of the minor, DMPG-enriched membrane component narrowed considerably. This result indicates a preferential interaction with net-negatively charged lipid membranes, and suggests that electrostatics play an important role in the interaction between cupiennin 1a and bacterial cell membranes. Given the cationic nature of the peptide, this is not surprising but is notably greater than previously reported for basic proteins (*72*). Changes in the ^{31}P chemical shift can be related to the surface charge density of the membrane (*54*), with decreasing negative charge density causing a small upfield shift. An upfield shift of 0.1−0.2 ppm was observed in the ^{31}P MAS spectra upon addition of cupiennin 1a only for the mixed-

DMPC/DMPG model membrane system, thereby further implicating the presence of cupiennin 1a for negatively charged membrane surfaces. These shifts are greater than those observed by Grobner and co-workers (*54*) for Aβ40 with DMPC/DMPG bilayers, which is consistent with the greater positive charge of cupiennin 1a.

Upon addition of cupiennin 1a, for each component of the mixed DMPC/DMPG MLV, T_1 and T_2 relaxation times lengthened. In contrast to the effect of the peptide on pure-DMPC MLV, this corresponds to a reduction in motions at the $\sim 10^8$ Hz and slow time scales, possibly due to changes in the fast axial rotation and collective motions of the lipids, respectively. The anisotropic motion of the phospholipid headgroup that dominates ^{31}P-T_1 relaxation exhibits a correlation time near a nanosecond (*64*). Therefore, T_1 can lengthen by either a reduction or an increase in correlation time since this system is very near its T_1 minimum already. Thus the increase in T_2 can be mostly explained by changes in T_1 processes, suggesting a shorter correlation time and, hence, the contribution of collective motions to these changes is highly unlikely. The changes in T_1 and T_2 are most likely due to changes in the fast axial rotation and indicate a strong interaction between the peptide and DMPC/DMPG phospholipids (*28*). The relative similarity in relaxation times between the DMPC- and DMPG-enriched components, in contrast to the differential observed in CSA, indicates that the components were distributed with respect to each other as very small domains, i.e., the DMPG-enriched component is unlikely to be segregated together with peptide in a single large domain on the MLV. Notably, upon association with peptide, the DMPG-enriched component revealed a narrowed CSA usually associated with increased head group mobility or a change in headgroup conformation (*49*), while the measured relaxation times suggest a relative reduction in mobility, albeit at different frequencies. The reduced CSA reports on changes in rotation of the phospholipid headgroup about the glycerol and the lipid long axis or an increase in the amplitude of wobble of the molecule about the bilayer normal (*49*). Diffusion over the surface of a planar lipid bilayer or MLV is too slow to cause the observed narrowing and would require a correlation time for the diffusion less than 100 μs (*49*). One explanation is that the reduced CSA is reporting on averaging of the shielding tensor between a planar and a more highly curved region. The differential effect observed at different time scales suggests a disruption to the bilayer structure and formation of a toroidal pore with the DMPG-enriched component lining the lumen formed by the peptide, similar to that described by Huang and co-workers for melittin (*73*).

When a peptide is incorporated in the bilayer surface (or interfacial) region, it may act as a spacer between the lipid head groups and provide more freedom of movement for the acyl chains, thereby decreasing their order (*74*, *75*). Since no disordering effect of cupiennin 1a was apparent by ^{2}H NMR over the entire acyl chain, it appears unlikely that this peptide adopts a predominantly surface orientation by inserting into the interface between the head groups and the chains in either zwitterionic or anionic lipids. This again is consistent with examples such as melittin, which can associate with phospholipid bilayers as a transmembrane helix, yet show limited perturbation of the lipids by solid-state NMR (*76*). The behavior of cupiennin 1a contrasts with that of shorter linear peptides ($\sim$25 residues) isolated from the venom of the *Lachesana tarabaevi* spider, Latarcins (Ltc), which exhibit broad-spectrum antibacterial activity. A recent NMR study found Ltc2a to have a similar helix−hinge−helix structural motif, but the peptide was only weakly amphiphilic (*77*). In addition, ^{31}P NMR data of the effect of the peptide on phospholipid liposomes, leading to a broad isotopic peak, suggests the carpet mechanism for membrane destabilization by Ltc2a. Cupiennin 1a, however, led to formation of two ^{31}P CSA, indicating formation of PC and PG enriched domains.

Based on the solution structures calculated in this study, the length of the N-terminal helix of cupiennin 1a is close to 30 Å, which is also the average thickness of a bacterial cell membrane (*78*) or PC bilayer (*79*). The length of this helix is, therefore, sufficient to span the bilayer, and therefore, we propose a pore-forming mechanism in which this segment would adopt a transmembrane orientation. Such a pore may be of the toroidal type, as described for melittin (*73*), which would account for the significant perturbation of the lipid head group region as indicated by ^{31}P NMR spectra of the anionic lipid MLV. However, as for the case of melittin (*73*), the mode of interaction may depend on several factors including the peptide/lipid ratio, lipid type, sample hydration, and temperature.

The mechanism by which cupiennin 1a induces cell lysis is subtly different in neutral and charged membranes, and the strong interaction between cupiennin 1a and anionic lipids may account for the observed specificity of this peptide, whereby the antibacterial efficacy is significantly more pronounced than the hemolytic activity. The extent to which the observed differences correspond to different modes of interactions with prokaryotic and eukaryotic membranes is not clear and invites further investigation. In conclusion, we propose that in neutral membranes, the amphipathic N-terminal helix of cupiennin 1a becomes buried within the core of the bilayer, acting as a driving force for pore formation and membrane disruption. In contrast, electrostatic interactions between the polar C-terminal helix and the anionic lipid head groups are anticipated to significantly disrupt the cell surface of charged membranes. The flexible hinge region of the peptide possibly may allow for the C-terminal portion to remain as an effective anchor at the membrane surface, while the N-terminal domain inserts into the hydrophobic region of the bilayer to form a structured pore.

SUPPORTING INFORMATION AVAILABLE

Additional information regarding the NMR structural characterization of cupiennin 1a and ^{2}H NMR data. This material is available free of charge via the Internet at http://pubs.acs.org.

REFERENCES

1. Nissen-Meyer, J., and Nes, I. F. (1997) Ribosomally synthesized antimicrobial peptides: their function, structure, biogenesis, and mechanism of action, *Arch. Microbiol. 167*, 67−77.
2. Boman, H. G. (1995) Peptide antibiotics and their role in innate immunity, *Annu. Rev. Immunol. 13*, 91−92.
3. Smet, K., and Contreras, R. (2005) Human antimicrobial peptides: Defensins, cathelicidins and histatins, *Biotechnol. Lett. 27*, 1337−1347.

4. Mazel, D., and Davies, J. (1999) Antibiotic resistance in microbes, *Cell. Mol. Life Sci. 56*, 742−754.
5. Bechinger, B. (1997) Structure and functions of channel-forming peptides—magainins, cecropins, melittin and alamethicin, *J. Membr. Biol. 156*, 197−211.
6. Epand, R. M., Shai, Y. C., Segrest, J. P., and Anantharamaiah, G. M. (1995) Mechanisms for the modulation of membrane bilayer properties by amphipathic helical peptides, *Biopolymers 37*, 319−338.
7. Matsuzaki, K., Sugishita, K., and Miyajima, K. (1999) Interactions of an antimicrobial peptide, magainin 2, with lipopolysaccharide-containing liposomes as a model for outer membranes of Gram-negative bacteria, *FEBS Lett. 449*, 221−224.
8. Oren, Z., and Shai, Y. (1998) Mode of action of linear amphipathic α-helical antimicrobial peptides, *Biopolymers 47*, 451−463.
9. Tossi, A., Sandri, L., and Giangaspero, A. (2000) Amphipathic, α-helical antimicrobial peptides, *Biopolymers 55*, 4−30.
10. Ehrenstein, G., and Lecar, H. (1977) Electrically gated ionic channels in lipid bilayers, *Q. Rev. Biophys. 10*, 1−34.
11. Sansom, M. S. P. (1991) The biophysics of peptide models of ion channels, *Prog. Biophys. Mol. Biol. 55*, 139−235.
12. Shai, Y. (1999) Mechanism of the binding, insertion and destabilization of phospholipid bilayer membranes by α-helical antimicrobial and cell non-selective membrane-lytic peptides, *Biochim. Biophys. Acta 1462*, 55−70.
13. Matsuzaki, K. (1999) Why and how are peptide-lipid interactions utilized for self-defense? Magainins and tachyplesins as archetypes, *Biochim. Biophys. Acta 1462*, 1−10.
14. Shai, Y., and Oren, Z. (2001) From "carpet" mechanism to de-novo designed diastereomeric cell-selective antimicrobial peptides, *Peptides 22*, 1629−1641.
15. Kuhn-Nentwig, L. (2003) Antimicrobial and cytolytic peptides of venomous arthropods, *Cell. Mol. Life Sci. 60*, 2651−2668.
16. Bernheimer, A. W., and Rudy, B. (1985) Interactions between membranes and cytolytic peptides, *Biochim. Biophys. Acta 864*, 123−141.
17. Verdonk, F., Bosteels, S., Desmet, J., Moerman, L., Noppe, W., Willems, J., Tytgat, J., and van der Walt, J. (2000) A novel class of pore-forming peptides in the venom of Parabuthus schlechteri Percell (Scorpions: Buthidae), *Cimbebasia 16*, 247−260.
18. Zeng, X., Corzo, G., and Hahin, R. (2005) Scorpion venom peptides without disulfide bridges, *IUBMB Life 57*, 13−21.
19. Kuhn-Nentwig, L., Schaller, J., and Nentwig, W. (2004) Biochemistry, toxicology and ecology of the venom of the spider *Cupiennius salei* (Ctenidae), *Toxicon 43*, 543−553.
20. Kuhn-Nentwig, L., Dathe, M., Walz, A., Schaller, J., and Nentwig, W. (2002) Cupiennin 1d*: The cytolytic activity depends on the hydrophobic N-terminus and is modulated by the polar C-terminus, *FEBS Lett. 527*, 193−198.
21. Kuhn-Nentwig, L., Müller, J., Schaller, J., Walz, A., Dathe, M., and Nentwig, W. (2002) Cupiennin 1, a new family of highly basic antimicrobial peptides in the venom of the spider *Cupiennius salei* (Ctenidae), *J. Biol. Chem. 277*, 11208−11216.
22. Evans, J. N. S. (1995) *Biomolecular NMR Spectroscopy*, Oxford University Press, Oxford.
23. Nilges, M., Macias, M. J., Odonoghue, S. I., and Oschkinat, H. (1997) Automated NOESY interpretation with ambiguous distance restraints—the refined NMR solution structure of the pleckstrin homology domain from *β*-spectrin, *J. Mol. Biol. 269*, 408−422.
24. Wider, G. (2000) Structure determination of biological macromolecules in solution using nuclear magnetic resonance spectroscopy, *Biotechniques 29*, 1278−1294.
25. Wüthrich, K., and Wider, G. (1982) Sequential resonance assignments as a basis for determination of spatial protein structures by high resolution proton nuclear magnetic resonance, *J. Mol. Biol. 155*, 311−319.
26. Bechinger, B. (2005) Detergent-like properties of magainin antibiotic peptides: a 31P solid-state NMR spectroscopy study, *Biochim. Biophys. Acta 1712*, 101−108.
27. Bechinger, B., Kinder, R., Helmle, M., Vogt, T. B., Harzer, U., and Schinzel, S. (1999) Peptide structural analysis by solid-state NMR spectroscopy, *Biopolymers 51*, 174−190.
28. Lu, J., Damodaran, K., Blazyk, J., and Lorigan, G. A. (2005) Solid-state nuclear magnetic resonance relaxation studies of the interaction mechanism of antimicrobial peptides with phospholipid bilayer systems, *Biochemistry 44*, 10208−10217.
29. Watts, A. (1998) Solid-state NMR approaches for studying the interaction of peptides and proteins with membranes, *Biochim. Biophys. Acta 1376*, 297−318.
30. Bloom, M., and Sternin, E. (1987) Transverse nuclear spin relaxation in phospholipid bilayer membranes, *Biochemistry 26*, 2101−2105.
31. Cornell, B. A., Hiller, R. G., Raison, J., Separovic, F., Smith, R., Vary, J. C., and Morris, C. (1983) Biological membranes are rich in low-frequency motion, *Biochim. Biophys. Acta 732*, 473−478.
32. Pinheiro, T. J. T., Duer, M. J., and Watts, A. (1997) Phospholipid headgroup dynamics in DOPG-d5-cytochrome C complexes as revealed by ^{2}H and ^{31}P NMR: The effects of a peripheral protein on collective lipid fluctuations, *Solid State NMR 8*, 55−64.
33. John, B. K., Plant, D., Webb, P., and Hurd, R. E. (1992) Effective combination of gradients and crafted RF pulses for water suppression in biological samples, *J. Magn. Reson. 98*, 200−206.
34. Griesinger, C., Otting, G., Wüthrich, K., and Ernst, R. R. (1988) Clean TOCSY for ^{1}H spin system identification in macromolecules, *J. Am. Chem. Soc. 110*, 7870−7872.
35. Wüthrich, K. (1986) *NMR of Proteins and Nucleic Acids*, John Wiley and Sons, New York.
36. Linge, J. P., Habeck, M., Rieping, W., and Nilges, M. (2003) ARIA: Automated NOE assignment and NMR structure calculation, *Bioinformatics 19*, 315−316.
37. Brünger, A. T. (1988) Crystallographic refinement by simulated annealing—application to a 2.8 Å resolution structure of aspartate aminotransferase, *J. Mol. Biol. 203*, 803−816.
38. Folmer, R. H. A., Hilbers, C. W., Konings, R. N. H., and Nilges, M. (1997) Floating stereospecific assignment revisited—application to an 18 kDa protein and comparison with J-coupling data, *J. Biomol. NMR 9*, 245−258.
39. Pari, K., Mueller, G. A., DeRose, E. F., Kirby, T. W., and London, R. E. (2003) Solution structure of the RNase H domain of the HIV-1 reverse transcriptase in the presence of magnesium, *Biochemistry 42*, 639−650.
40. Koradi, R., Billeter, M., and Wüthrich, K. (1996) MOLMOL—a program for display and analysis of macromolecular structures, *J. Mol. Graphics 14*, 51−55.
41. Mehring, M. (1983) *Principles of High Resolution NMR in Solids*, Springer-Verlag, Berlin.
42. Pott, T., and Dufourc, E. J. (1995) Action of melittin on the DPPC-cholesterol liquid-ordered phase: A solid-state ^{2}H- and ^{31}P-NMR study, *Biophys. J. 68*, 965−977.
43. Davis, J. H., Jeffrey, K. R., Bloom, M., Valic, M. I., and Higgs, T. P. (1976) Quadrupolar echo deuteron magnetic resonance spectroscopy in ordered hydrocarbon chains, *Chem. Phys. Lett. 42*, 390−394.
44. Galassi, M., Davies, J., Theiler, J., Gough, B., Jungman, G., Booth, M., and F., R. *GNU Scientific Library Reference Manual*, revised 2nd ed. ISBN 0954161734, http://www.gnu.org.software/gsl/.
45. Wishart, D. S., Bigam, C. G., Holm, A., Hodges, R. S., and Sykes, B. D. (1995) H-1, C-13 and N-15 random coil NMR chemical shifts of the common amino acids. 1. Investigations of nearest-neighbor effects, *J. Biomol. NMR 5*, 67−81.
46. Wishart, D. S., Sykes, B. D., and Richards, F. M. (1991) Relationship between nuclear magnetic resonance chemical shift and protein secondary structure, *J. Mol. Biol. 222*, 311−333.
47. Zhou, N. E., Zhu, B., Sykes, B. D., and Hodges, R. S. (1992) Relationship between amide proton chemical shifts and hydrogen bonding in amphipathic α-helical peptides, *J. Am. Chem. Soc. 114*, 4320−4326.
48. Seelig, J. (1978) ^{31}P nuclear magnetic resonance and the head group structure of phospholipids in membranes, *Biochim. Biophys. Acta 515*, 105−140.
49. Kohler, S. J., and Klein, M. P. (1977) Orientation and dynamics of phospholipid head groups in bilayers and membranes determined from ^{31}P nuclear magnetic resonance chemical shielding tensors, *Biochemistry 16*, 519−526.
50. Seelig, J., and Seelig, A. (1980) Lipid conformation in model membranes and biological membranes, *Q. Rev. Biophys. 13*, 19−61.
51. Bechinger, B. (2000) Biophysical investigations of membrane perturbations by polypeptides using solid-state NMR spectroscopy (review), *Mol. Membr. Biol. 17*, 135−142.
52. Scherer, P. G., and Seelig, J. (1989) Electric charge effects on phospholipid headgroups. Phosphatidylcholine in mixtures with cationic and anionic amphiphiles, *Biochemistry 28*, 7720−7728.
53. Balla, M. S., Bowie, J. H., and Separovic, F. (2004) Solid-state NMR study of antimicrobial peptides from Australian frogs in phospholipid membranes, *Eur. Biophys. J. 33*, 109−116.
54. Bonev, B., Watts, A., Bokvist, M., and Grobner, G. (2001) Electrostatic peptide-lipid interactions of amyloid-*β* peptide and

pentalysine with membrane surfaces monitored by ^{31}P MAS NMR, *Phys. Chem. Chem. Phys. 3*, 2904−2910.
55. Seelig, A., and Seelig, J. (1974) The dynamic structure of fatty acyl chains in a phospholipid bilayer measured by deuterium magnetic resonance, *Biochemistry 13*, 4839−4845.
56. Boden, N., Jones, S. A., and Sixl, F. (1991) On the use of deuterium nuclear magetic resonance as a probe of chain packing in lipid bilayers, *Biochemistry 30*, 2146−2155.
57. Davis, J. H. (1983) The description of membrane lipid conformation, order and dynamics by ^{2}H-NMR, *Biochim. Biophys. Acta 737*, 117−171.
58. Lafleur, M., Fine, B., Sternin, E., Cullis, P. R., and Bloom, M. (1989) Smoothed orientational order profile of lipid bilayers by ^{2}H-nuclear magnetic resonance, *Biophys. J. 56*, 1037−1041.
59. Otten, D., Brown, M. F., and Beyer, K. (2000) Softening of membrane bilayers by detergents elucidated by deuterium NMR spectroscopy, *J. Phys. Chem. 104*, 12119−12129.
60. Lu, D., Vavasour, I., and Morrow, M. R. (1995) Smoothed acyl chain orientational order parameter profiles in dimyristoylphosphatidylcholine-distearoylphosphatidylcholine mixtures: a 2H-NMR study, *Biophys. J. 68*, 574−583.
61. Dvinskikh, S. V., Castro, V., and Sandstrom, D. (2005) Probing segmental order in lipid bilayers at variable hydration levels by amplitude- and phase-modulated cross-polarization NMR, *Phys. Chem. Chem. Phys. 7*, 3255−3257.
62. Andrew, E. G., Bradbury, A., and Eades, R. G. (1959) Removal of dipolar broadening of nuclear magnetic resonance spectra of solids by specimen rotation, *Nature 183*, 1802−1803.
63. Davis, J. H., and Auger, M. (1999) Static and magic angle spinning NMR of membrane peptides and proteins, *Prog. Nucl. Magn. Reson. Spectrosc. 35*, 1−84.
64. Yeagle, P. L., Hutton, W. C., Huang, C.-H., and Martin, R. B. (1975) Headgroup conformation and lipid-cholesterol association in phosphatidylcholine vesicles: A ^{31}P{^{1}H} nuclear Overhauser effect study, *Proc. Natl. Acad. Sci. U.S.A. 72*, 3477−3481.
65. Separovic, F., Cornell, B. A., and Pace, R. (2000) Orientation dependence of NMR relaxation time, $T_{1\rho}$, in lipid bilayers, *Chem. Phys. Lipids 107*, 159−167.
66. Rajan, R., and Balaram, P. (1996) A model for the interaction of trifluoroethanol with peptides and proteins, *Int. J. Pept. Protein Res. 48*, 328−336.
67. Hirota, N., Mizuno, K., and Goto, Y. (1998) Group additive contributions to the alcohol-induced alpha-helix formation of melittin—implication for the mechanism of the alcohol effects on proteins, *J. Mol. Biol. 275*, 365−378.
68. Rizo, J., Blanco, F. J., Kobe, B., Bruch, M. D., and Gierasch, L. M. (1993) Conformational behavior of *Escherichia coli* OmpA signal peptides in membrane mimetic environments, *Biochemistry 32*, 4881−4894.
69. Gesell, J., Zasloff, M., and Opella, S. J. (1997) Two-dimensional ^{1}H NMR experiments show that the 23-residue magainin antibiotic peptide is an alpha-helix in dodecylphosphocholine micelles, sodium dodecylsulfate micelles, and trifluoroethanol/water solution, *J. Biomol. NMR 9*, 127−135.
70. Woolfson, D. N., and Williams, D. H. (1990) The influence of proline residues on α-helical structure, *FEBS Lett. 277*, 185−188.
71. Gunasekaran, K., Nagarajam, H. A., Ramakrishnan, C., and Balaram, P. (1998) Stereochemical punctuation marks in protein structures: glycine and proline containing helix stop signals, *J. Mol. Biol. 275*, 917−932.
72. Smith, R., Cornell, B. A., Keniry, M. A., and Separovic, F. (1983) 31P nuclear magnetic resonance studies of the association of basic proteins with multilayers of diacyl phosphatidylserine, *Biochim. Biophys. Acta 732*, 492−498.
73. Yang, L., Harroun, T. A., Weiss, T. M., Dong, L., and Huang, H. W. (2001) Barrel-stave model or toroidal model? A case study on melittin pores, *Biophys. J. 81*, 1475−1485.
74. Strandberg, E., and Ulrich, A. S. (2004) NMR methods for studying membrane-active antimicrobial peptides, *Concepts Magn. Reson. A 23*, 89−120.
75. Yamaguchi, S., Huster, D., Waring, A., Lehrer, R. I., Kearney, W., Tack, B. F., and Hong, M. (2001) Orientation and dynamics of an antimicrobial peptide in the lipid bilayer by solid-state NMR spectroscopy, *Biophys. J. 81*, 2203−2214.
76. Smith, R., Separovic, F., Bennett, F. C., and Cornell, B. A. (1992) Melittin-induced changes in lipid multilayers, *Biophys. J. 63*, 469−474.
77. Dubovski, P. V., Volynsky, P. E., Polyansky, A. A., Chupin, V. V., Efremov, R. G., and Arseniev, A. S. (2006) Spatial structure and activity mechanism of a novel spider antimicrobial petpide, *Biochemistry 45*, 10759−10767.
78. Brock, T. D. (1984) *Biology of Microorganisms*, 4th ed., Prentice Hall Inc., Englewood Cliffs.
79. Cornell, B. A., and Separovic, F. (1983) Membrane thickness and acyl chain length, *Biochim. Biophys. Acta 733*, 189−193.

BI062306+